HAC2018 | V Congreso Iberoamericano de Hormigón Autocompactante y Hormigones Especiales

Valencia, 5 y 6 de Marzo de 2018

Ultra High Performance Concrete - Materials Formulations and Serviceability based Design

Yiming Yao [(1)], Aashay Arora [(2)], Narayanan Neithalath [(3)] and Barzin Mobasher [(3)]

[(1)] Associate Professor, Southeast University, Nanjing, Jiangsu, China.

[(1)] Graduate Research Assistant, School of Sustainable Engineering and the Built Environment, Arizona State University, Tempe, AZ, USA.

[(2)] Professor, School of Sustainable Engineering and the Built Environment, Arizona State University, Tempe, AZ, USA.

DOI: http://dx.doi.org/10.4995/HAC2018.2018.8263

ABSTRACT

Materials and mechanical design procedures for ultra-high performance cement composites (UHPC) members based on analytical models are addressed. A procedure for the design of blended components of UHPC is proposed using quaternary cementitious materials. The blending procedures are used using a packing and rheology optimization approach to blend high performance mixtures using non-proprietary formulations. Closed-form solutions of moment-curvature responses of UHPC are derived based on elastic-plastic compressive model and trilinear strain hardening tension stress strain responses. Tension stiffening behavior of UHPC due to fiber toughening and distributed cracking is then incorporated in the cross-sectional analysis. Load-deflection responses for beam members are obtained using moment-area, and direct integration approach. The proposed models provide insights in the design of SHCC to utilize the hardening properties after cracking. Using proper parameters, generalized materials model developed are applicable to both SHCC and strain softening cement composites such as steel fiber reinforced concrete (SFRC), textile reinforced concrete (TRC) and ultra-high performance concrete (UHPC).

KEYWORDS: Strain hardening cement composites, distributed cracking, textile reinforced concrete, strain hardening, design.

1.- INTRODUCTION

Strain hardening cement composite (UHPC) is a class of materials using relatively high fiber volume fraction (more than 2%) and exhibiting high strength and ductility. In contrast to conventional concrete, increases in tensile stresses are observed after first crack in tension through crack bridging and interface transfer mechanisms provided by discrete fibers. The UHPC class requires a fundamental concentration on the matrix phase and its rheology in order to achieve high compressive strength and ductility. The durability of

concrete structures improves as a result of crack mitigation, where discrete cracks are replaced with a system of distributed micro cracks.

UHPC is an ideal construction material for applications that require rapid construction and connection of precast segments, applications that require a reduction of the weight and size of structure, or for seismic design where high ductility is desired. Figure 1 shows the application of UHPC connection between precast deck panels [Greybeal, 2014]. The improved performance of SHCCs subjected fatigue and impact loads make them attractive for industrial structures, highway pavements, bridges, and natural hazardous and extreme loads. In contrast to the design of conventional RC structures, implementation of UHPC requires use of strain-hardening response that is attributed to multiple cracking due to load transfer by the fibers across the cracks (Mobasher et al. 2006b). As multiple cracking takes place, the stiffness of the sample significantly drops while the crack spacing continuously decreases to a saturation level. The post crack stiffness and the ultimate strain capacity are functions of fiber type, stiffness, and bonding characteristics, however the stiffness in the post crack region can be effectively used in the analytical and design formulations (Mobasher et al. 2006a).

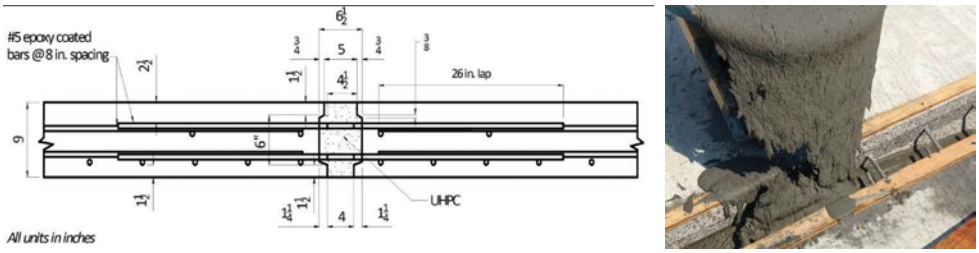

Figure 1. UHPC connection between precast deck panels as deployed by NYSDOT on I-81 in Syracuse, NY [Greybeal,2014]

2.- MATERIALS DEVELOPMENT

The main objective is by controlled blending of components with up to 3% volume fraction of steel fibers, a UHPC formulation can be obtained with non-proprietary materials that is strong, ductile, and durable. A systematic procedure was developed for a multiple (up to four component) non-proprietary paste components that can be blended for optimal performance. This paste system constitutes the main component of UHPC formulation, when used with specifically blended and sized aggregates of specified particle size distribution, it would yield the UHPC system.

Figure 2 shows the strategy to obtain the optimized design of UHPC. The research approach is built around three fundamental steps: binder (paste) design, aggregate packing and optimization, and testing the final properties. The binder design, shown in Figure 2 consists of selection of the source materials for the binder from a series of common cementing (or cement replacement) materials. Ordinary Portland cement (OPC), Flyash, (F), MicroSilica, (M), Slag, (S), Metakaolin, (K), Limestone, (La, Lb, 3.0 and 1.5 micron).

Different properties of the microstructure can be analyzed using the 3D particle packing models. 3D volumes are generated using a stochastic particle packing model assuming spherical particles.

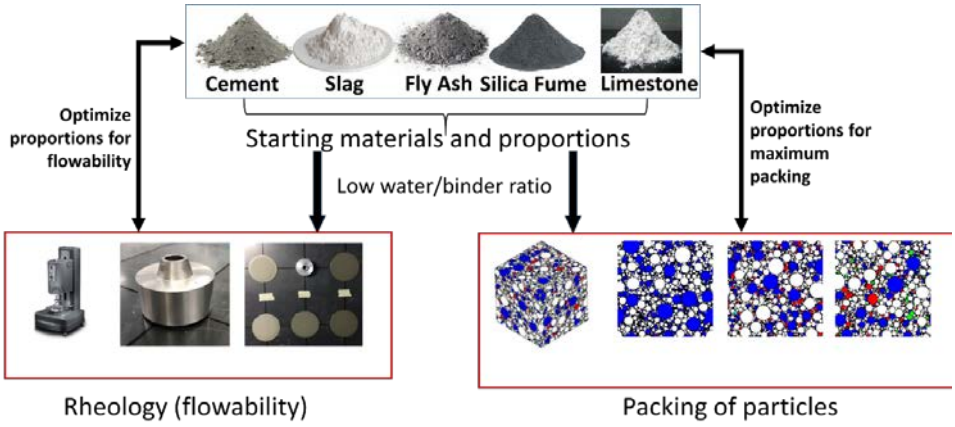

Figure 2. Schematic showing the aggregate packing of UHPC

The goal is to use a blend of the cementitious materials that can be mixed with a very low w/b ratio and, with the aid of superplasticizers, can result in flowable and workable mixtures. The microstructural packing and rheological studies provide preliminary indicators as to the applicability of paste systems for UHPC. Packing influences rheology and mechanical/durability properties, while rheology influences placing and early-age structure development, which in turn influences the later age properties. In a composite binder that contains particles of different size distributions and surface characteristics, chemical admixtures are essential in controlling the rheological features. One would start with the materials (cement, fly ash, silica fume etc.) with particle sizes ranging from 0.1 microns to 50 microns. Therefore F20L10b would indicate a blended composite cement with 20% Flyash and 10% Limestone. The selected components and their mass fractions are combined to ensure maximum packing of the powder ingredients. The flowability of the binders at very low w/b, and in the presence of large amounts of chemical admixtures are evaluated using fundamental rheological experiments.

In the second step, the optimized packing of selected coarse and fine aggregates and fibers are tested to meet the performance criteria. Selection of aggregates is based on a compressible packing model (CPM) which determines the maximum packing density using different sizes of coarse and fine aggregates. The packing efficiency reduces the capillary pores and therefore improves the strength and the impermeability significantly. This is shown in Figure 3(a). The finalized UHPC mixture(s) are then subjected to property-and-performance testing that includes mechanical testing (compression, tension, flexural, fracture) and durability evaluation (resistance to freezing and thawing, chloride penetration). This approach shows that UHPC concrete mixtures can be developed using locally obtained materials. [Arora et. al, 2017]

2.1.- Strength and Fracture response

Figure 3(b) shows the compressive strengths of mortars made using the selected UHP pastes after 14 and 28 days of moist curing. Even with a clinker factor reduction of 30%, the UHP mortars, especially the quaternary blends demonstrate 28 day strengths that are comparable to, or higher than that of the control UHP mortar. The mixtures containing slag demonstrate higher strengths than those containing fly ash at 28 days, but it is conceivable that the pozzolanic reaction of fly ash and its later synergy with the other replacement materials could improve the strength with further curing. It is noted that the addition of fibers, reduction of water to binder ratio, optimization of the aggregate size fractions would lead to a final mixture with 28 day compressive strengths in excess of 22,000 psi (150 MPa).

The flexural response results are shown in Figure 4. Note that the increase in strength by means of microsctructural modification is also complimentary to the role of fibers in increasing the load carrying resistance and the strength hand ductility are both improved with the use of steel fibers. Figure 4.b shows the digital image correlation of the formation of multiple cracks in the flexural samples at various stages.

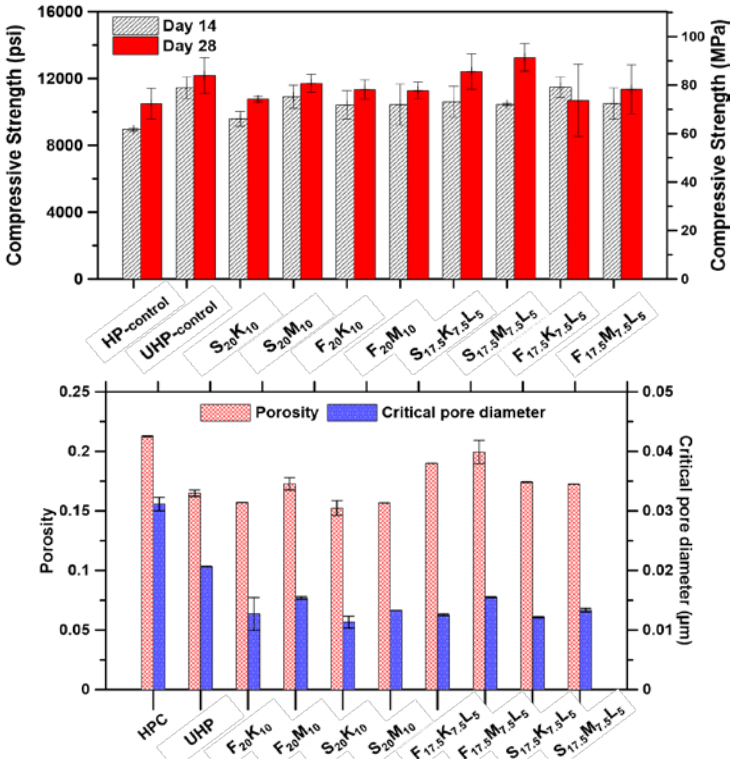

Figure 3. a) Mercury intrusion porosity and critical pore diameters for selected UHPC specimens b) compressive strengths at Day 14 and day 28 of selected UHP mortars.

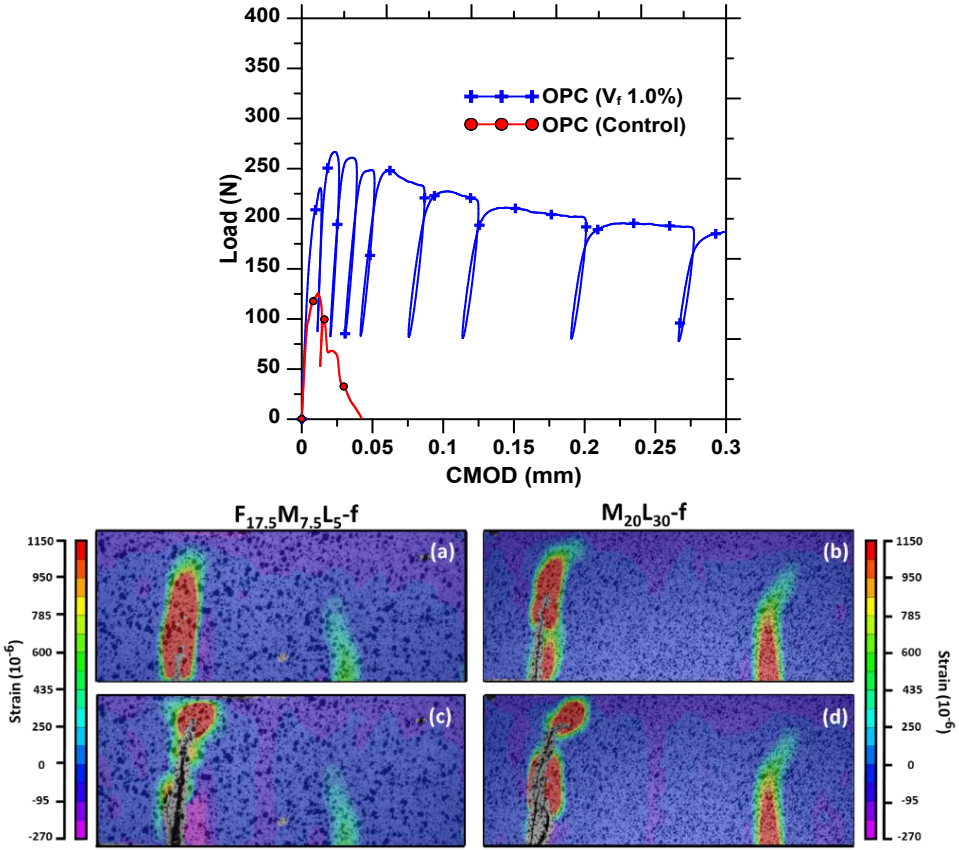

Figure 4. a) load vs. CMOD for control fiber reinforced beam specimens with 1% steel fiber at a post peak stress of (a,b) 90% and (c,d) 50% of the peak stress.

2.2.- Modeling and Structural Design of Strain-Hardening Composites

A broad range of cement composites exhibiting strain-hardening behavior can be modelled using the proposed approach. These materials include textile reinforced concrete (TRC), fiber reinforced concrete (FRC), and ultra-high performance fiber reinforced concrete (UHPC). The general behavior can be simulated by linearized compression and tension models that address nonlinear and hardening properties as shown in Figure 5 (Soranakom and Mobasher 2008). Tensile response is defined by Young's Modulus E, first crack tensile strain ε_{cr}, transition strain ε_{trn}, and post crack modulus E_{cr}. Note that by normalizing all parameters by minimum number of independent and dimensionless variables, tensile response uses only two intrinsic material parameters E and ε_{cr}, therefore the softening or residual range is defined by a constant stress level $\mu E\varepsilon_{cr}$, and the compressive strength $\sigma_{cy}= \omega\gamma E\varepsilon_{cr}$. Other material parameters are summarized as follows: α, μ, η, ω and defined

respectively as normalized tensile strain at peak strength, residual tensile strength, post-crack modulus, and compressive yield strength (Soranakom and Mobasher 2008).

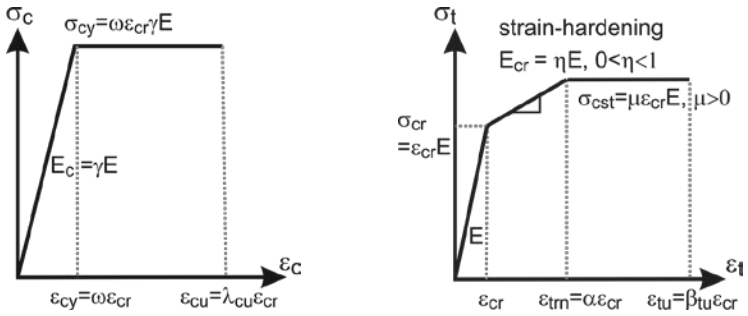

Figure 5. Material model for SHCC (a) compression, (b) tension model (Yao et al. 2017).

Even though the tensile strength is greatly improved in SHCC, the compressive strength in is still much higher, and the flexural capacity is defined by means of the tensile variable. The nonlinearity and failure in flexure are likely to be dominated by tensile properties. One can perform cross-sectional analysis by constructing strain and stress profiles. Followed by integration of normal stresses, the compressive and tensile force terms from each zone are obtained and bending moment on the cross section computed. Closed-form solutions of moment-curvature responses are explicitly derived based on interactions among different stages in tension and compression models. The detailed derivations for strain softening, strain hardening FRC as well as hybrid reinforced concrete (HRC) sections containing rebar and fibers can be found in (Mobasher et al. 2015; Soranakom and Mobasher 2008). These equations can be further simplified using polynomial or power curve fitting with detailed applications for individual cases presented in (Yao et al. 2017).

The solution for the plain fiber reinforced concrete section is presented first. For the given applied strain distribution, the location of neutral axis, defined as *kd* is obtained from the force equilibrium equations. For a specified serviceability limit based on maximum allowable compressive strain $\varepsilon_c = \lambda_{cu}\ \varepsilon_{cr}$, the neutral axis depth and the bending moment are obtained as:

$$k = \frac{2\mu\lambda_{cu}}{-\omega^2 + 2\lambda_{cu}(\omega+\mu) + 2\mu - 1} \tag{1}$$

$$M_n = \left(\left(3\omega\lambda_{cu}^2 - \omega^3 + 3\mu\lambda_{cu}^2 - 3\mu + 2\right)\frac{k^2}{\lambda_{cu}^2} - 3\mu\left(2k-1\right) \right) M_{cr} \tag{2}$$

$$M_{cr} = \frac{\sigma_{cr} b h^2}{6} \tag{3}$$

On may conduct an asymptotic analysis to compute the moment capacity in the limit case, a simplified design equation for normalized moment capacity is obtained. This resembles a case when the cracked section in flexure opens significantly to go beyond serviceability limit, however due to the presence of fibers, the section can still transmit the flexural load applied. The moment capacity in this case is defined by the limit case of compressive cracking strain λ_{cu} reaching a relatively large number [1]. To further simplify Equation 2, The residual strength of FRC in flexure is approximately three times its residual strength in tension, that is, $f_{eq,3} = 3\mu\sigma_{cr}$ [ACI-544-8R [6], M_n. Furthermore, the empirical relationship between tensile and compressive strength $f_t' = 6.7\sqrt{f_c'}$ (in U.S. customary units) is used for normalized compressive strength ω:

$$\omega = \frac{\gamma E \omega \varepsilon_{cr}}{E\varepsilon_{cr}} \approx \begin{cases} \dfrac{f_c'}{f_t'} = \dfrac{0.85 f_c'}{6.7\sqrt{f_c'}} = 0.127\sqrt{f_c'} & (f_c' \text{ in psi}) \\ \dfrac{f_c'}{f_t'} = \dfrac{0.85 f_c'}{0.56\sqrt{f_c'}} = 1.518\sqrt{f_c'} & (f_c' \text{ in MPa}) \end{cases} \tag{4}$$

By substituting for ω, as a function of ultimate compressive strength f_c' and the post crack tensile strength μ the expression for nominal ultimate moment capacity is obtained.

$$M_n = \left[\frac{6 f_{eq,3}\sqrt{f_c'}}{\xi(f_{eq,3} + 3f_c')} \right] M_{cr}, \qquad \xi = 15.8 \text{ for U.S. units; } \xi = 1.32 \text{ for SI} \tag{5}$$

The ultimate moment capacity as a function of residual tensile strength and reinforcement can be used as a convenient design tool for combinations of reinforcements, calculated as shown in Eq. (6). An analytical expression for minimum reinforcement ratio $\rho_{g,min}$ for conventional reinforced concrete is obtained. For example, using parameters $\mu = 0$, $\gamma = 3/4$, and $\omega = 6$, Eq. (7) represents the minimum reinforcement as a function of location and its stiffness (steel or FRP).

$$M_n \approx m_\infty M_{cr} = \frac{6\rho_g n\kappa(\mu\alpha - \mu + \alpha\omega) + 3\omega\mu - 3(\rho_g n\kappa)^2}{\omega + \mu} M_{cr} \tag{6}$$

$$\rho_{\min} = \frac{9\alpha - \sqrt{81\alpha^2 - 6}}{2\alpha n\kappa} \tag{7}$$

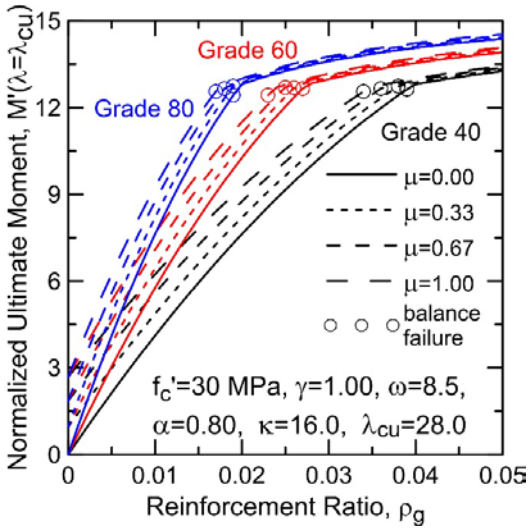

Figure 6. Design chart for normalized ultimate moment capacity (determined at $\lambda=\lambda_{cu}$) for different levels of post crack tensile strength μ and reinforcement ratio ρ_g..

Equations to determine the moment-curvature relationship, ultimate moment capacity, and minimum flexural reinforcement ratio were also explicitly derived by Yao et al (2018). Figure 6 shows a design chart for the parametric design model with various grades of steel. Flexural design using this chart, requires ultimate moment M_u due to factored loads normalized with respect to cross-sectional geometry. The demand moment capacity M_u' is obtained from this chart using a combination of normalized residual tensile strength μ, grade of steel, and reinforcement ratio ρ_g. Results are scaled to numerical values using the section cracking moment M_{cr}.

3.- MOMENT-CURVATURE AND LOAD-DEFLECTION RELATIONSHIPS

Moment-curvature relationship as cross sectional properties connects the constitutive material parameters to the structural flexural behavior, equilibrium, and the curvature-displacement relationship. This design parameter can be represented in various forms of bilinear, tri-linear, or curve fit from various sections (Soranakom and Mobasher 2008; Wang 2015). To obtain load-deflection calculations with given moment-curvature response, two approaches can be applied to the slope deflection equation: direct integration and polynomial/piecewise integration of linearized segments as discussed in (Soranakom and Mobasher 2008). Alternatively, one can use a parameterized moment-curvature relationship for a generalized solution, which has been derived and proposed as a practical design tool Wang (2015), Yao et al, (2018).

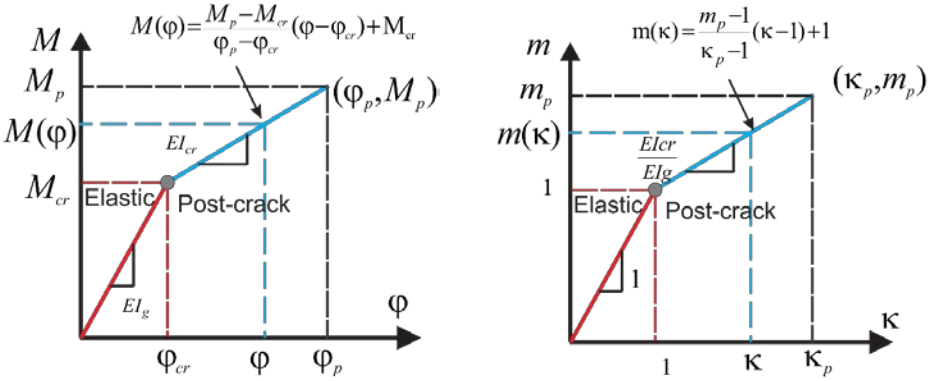

Figure 7. Simplified parametric moment-curvature relationship: (a) bilinear representation, (b) dimensionless moment-curvature curve represented as variables (κ, m).

Figure 7a and 7b presents the idealized parametric moment–curvature response of a deflection hardening case with a two stage linear elastic and a post-cracking range. The mid-span deflection is obtained directly using the double integration of curvature distribution and imposing boundary conditions to ensure the continuity of displacement fields (Wang 2015). Deflection distributions along the beams at full range of applied loads were derived for various beam types, loading conditions and supports such as simple beam, cantilever beam, point load/moment, distributed load and combination of them. Analytical expressions of the mid-span deflections for 3PB and 4PB are presented for elastic (Stage 1) and cracked (Stage 2) stages. where $L_e = a/m$ refers to the length of elastic region, and a is the shear span of 4PB beam.

3PB:

$$\delta_1 = -\frac{\kappa}{12}\varphi_{cr} L^2$$
$$\delta_2 = \frac{\varphi_{cr} L^2}{L-2L_e}\left[\frac{(\kappa-1)L}{24} + \frac{(2L_e - L)\kappa}{8} + \frac{L_e^2(L-2\kappa L_e)}{6L^2}\right] \quad (8)$$

4PB:

$$\delta_1 = \kappa\varphi_{cr}\left(\frac{a^2}{6} - \frac{L^2}{8}\right)$$
$$\delta_2 = \left\{\frac{1}{54}\left[\left(\frac{3L_e}{L}+1\right)\left(\frac{3\kappa L_e}{L}-1\right)+\kappa\right] - \frac{\kappa}{8}\right\}\varphi_{cr} L^2 \quad (9)$$

4.- MODEL SIMULATION

To verify the analytical model for flexural results of SHCC and UHPC beams studied by Qian and Li (2008), and Yoo et al. (2016) are simulated. Plain beam specimens of both SHCC and UHPC had a rectangular cross section of 100x100 mm2 and a span of 300 mm. Four-point bending tests were conducted and load and deflection responses were recorded. The compressive strength for the UHPC and SHCC specimens are 232 MPa and 46 MPa, respectively.

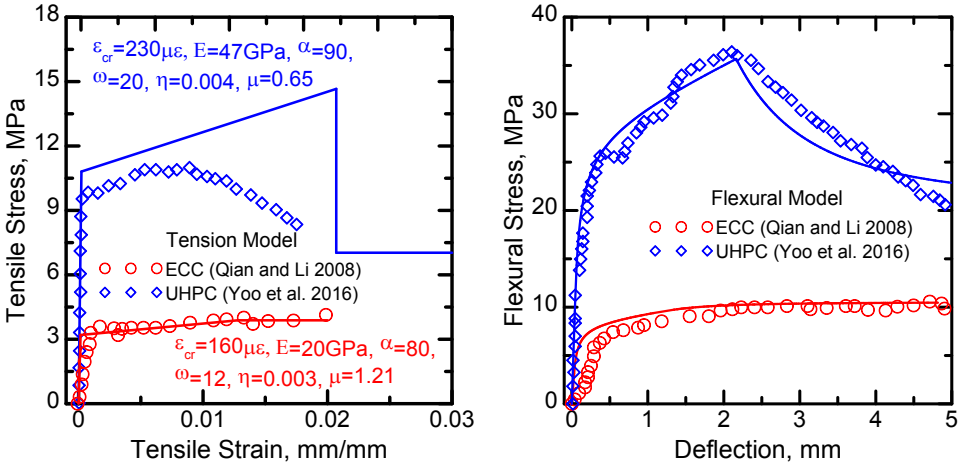

Figure 8. Simulations of ECC and UHPC specimens (a) tension models, (b) flexural stress-deflection responses.

Figures 8(a) and (b) compare the tensile stress-strain and flexural stress-deflection responses, respectively, for SHCC and UHPC composites. For SHCC, the model parameters include cracking strain ε_{cr}=160με, Young's modulus E=20GPa, normalized transition strain α=80, normalized compressive strength ω=12, post-cracking stiffness η=0.003. For UHPC specimens, these values are ε_{cr}=230με, E=47 GPa, α=90, ω=20, η=0.004, as indicated in Figure 8(a). Strain hardening was demonstrated in both systems while UHPC showed much higher crack and ultimate tensile strength due to improved matrix properties and use of steel fibers. Use of ductile PVA fibers in SHCC results in more pronounced ductility in tension and flexure. The tension models in Figure 8(a) are used to construct the moment-curvature relationship and the deflection equations. The applied load is obtained from static equilibrium of a 4PB beam while the mid-span deflections are obtained from curvature. The simulated load-deflection responses are compared with experimental results in Figure 8(b). Deflection hardening are showed by both materials in bending due to distributed flexural cracking. The analytical model agrees well with the experimental data.

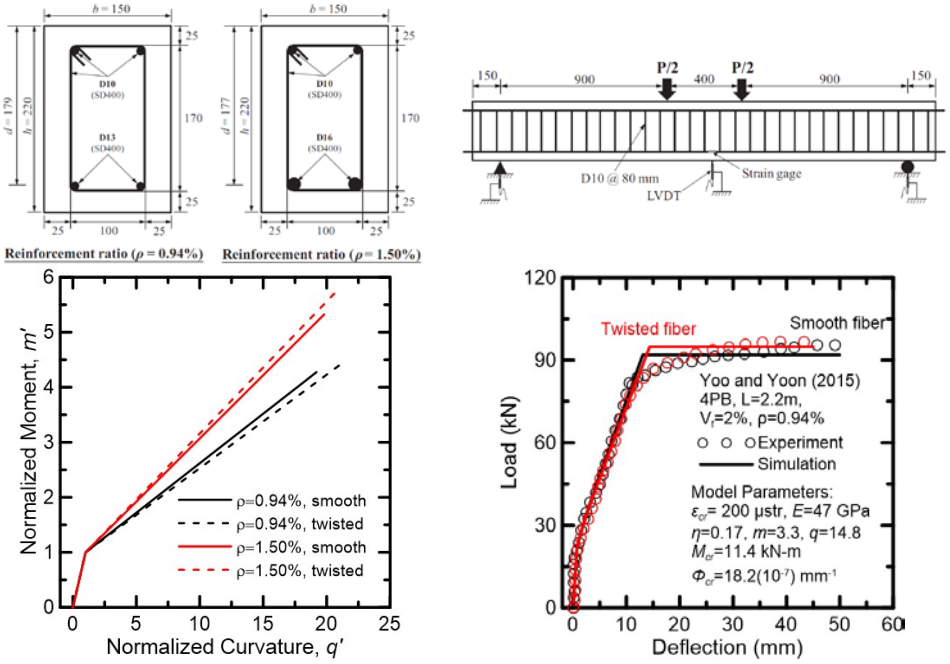

Figure 9. (a) Geometry of the cross section of UHPC beams, b) beam and loading geometry, c) Normalized moment-curvature relationship, d) comparison of load-deflection responses between simulation and experimental data for ρ=0.94%, and ρ=1.50%..

In the second simulation test results of hybrid reinforced concrete beams with UHPC and combinations of rebar and steel fiber tested by Yoo and Yoon, (2015). The beams with a cross section of 150 mm by 220 mm are tested under 4PB and span of 2200 mm are shown in Figures 9(a) and 9(b). Effect of longitudinal reinforcement ratio was evaluated at 0.94% and 1.50%. Two distinct types of smooth and twisted steel fibers at volume fraction of 2% were used. Figure 9(c) shows the normalized moment-curvature responses and Figure 9(d) compares the predicted and experimental load-deflection responses for of ρ=0.94% and 1.50%, respectively. The basic material parameters used in the model include Young's modulus E = 47GPa, first crack tensile strain ε_{cr} = 180$\mu\varepsilon$. Other model parameters shown in the Figure. Note that the proposed model provides conservative estimation for this class of materials, a preferred feature from the design perspective.

4.- CONCLUSIONS

A procedure for the design of blended components of UHPC was developed for using quaternary cementitious materials. The blending procedures use packing and rheology optimization approach to blend high performance mixtures using non-proprietary formulations. Tension hardening and multiple cracking behavior were obtained by the

deflection hardening mechanisms and energy dissipation in flexural members made with UHPC was documented. An analytical model based on serviceability limits for design of FRC and UHPC members is presented. Load-deflection responses are obtained using moment-area method or in closed-form by means of a linearized moment-curvature and double integration. The proposed models were verified by several experimental studies.

REFERENCES

Arora, A., Aguayo, M., Hansen, H., Castro, C., Federspiel, E., Mobasher, B., Neithalath, N., " Microstructural packing and rheology-based binder selection and characterization for Ultra-high Performance Concrete (UHPC)" , Cement and Concrete Research 103, 179-190, 2018

Aswani, K. (2014). "Design procedures for Strain Hardening Cement Composites (SHCC) and measurement of their shear properties by mechanical and 2-D Digital Image Correlation (DIC) method." Arizona State University, Master Thesis.

Facconi, L., Minelli, F., and Plizzari, G. (2016). "Steel fiber reinforced self-compacting concrete thin slabs – Experimental study and verification against Model Code 2010 provisions." *Engineering Structures*, 122, 226–237.

Graybeal, B. (2014). Design and construction of field-cast UHPC Connections (No. FHWA-HRT-14-084).

Johansen, K. W. (1962). *Yield-line theory*. Cement and Concrete Association, London.

Khaloo, A. R., and Afshari, M. (2005). "Flexural behaviour of small steel fibre reinforced concrete slabs." *Cement and Concrete Composites*, 27(1), 141–149.

Kim, J., Kim, D. J., Park, S. H., and Zi, G. (2015). "Investigating the flexural resistance of fiber reinforced cementitious composites under biaxial condition." *Composite Structures*, 122, 198–208.

Mobasher, B. (2011). Mechanics of Fiber and Textile Reinforced Cement Composites. CRC Press.

Mobasher, B., Pahilajani, J., and Peled, A. (2006a). "Analytical simulation of tensile response of fabric reinforced cement based composites." *Cement and Concrete Composites*, 28(1), 77–89.

Mobasher, B., Peled, A., and Pahilajani, J. (2006b). "Distributed cracking and stiffness degradation in fabric-cement composites." *Materials and Structures*, 39(3), 317–331.

Mobasher, B., Yao, Y., and Soranakom, C. (2015). "Analytical solutions for flexural design of hybrid steel fiber reinforced concrete beams." *Engineering Structures*, 100, 164–177.

Qian, S., and Li, V. C. (2008). "Simplified Inverse Method for Determining the Tensile Properties of Strain Hardening Cementitious Composites (SHCC)." *Journal of Advanced Concrete Technology*, 6(2), 353–363.

Sawyer, H. A. J. (1965). "Design of Concrete Frames For Two Failure Stages." *Special Publication*, 12, 405–437.

Soranakom, C., and Mobasher, B. (2008). "Correlation of tensile and flexural responses of strain softening and strain hardening cement composites." *Cement and Concrete Composites*, 30(6), 465–477.

Wang, X. (2015). "Analytical Load-Deflection Equations for Beam and 2-D Panel with a Bilinear Moment-Curvature Model." Master Thesis, ARIZONA STATE UNIVERSITY.

Yao, Y., Wang, X., Aswani, K., and Mobasher, B. (2017). "Analytical procedures for design of strain softening and hardening cement composites." *International Journal of Advances in Engineering Sciences and Applied Mathematics*, 1–14.

Yoo, D.-Y., Banthia, N., Kang, S.-T., and Yoon, Y.-S. (2016). "Size effect in ultra-high-performance concrete beams." *Engineering Fracture Mechanics*, 157, 86–106.

Yoo, D. Y., & Yoon, Y. S. (2015). Structural performance of ultra-high-performance concrete beams with different steel fibers."*Engineering Structures*,"*102*, 409-423.